Journal of Hydrology 609 (2022) 127757

Contents lists available at ScienceDirect

Journal of Hydrology

journal homepage: www.elsevier.com/locate/jhydrol

Research papers

The root-zone soil moisture spectrum in a mediterranean ecosystem

Roberto Corona [a,*], Gabriel Katul [b], Nicola Montaldo [a]

[a] Dipartimento di Ingegneria civile, ambientale e architecture, Universita di Cagliari, Cagliari, Italy
[b] Department of Civil and Environmental Engineering, Duke University, Durham, NC, USA

ARTICLE INFO

This manuscript was handled by Corrado Corradini, Editor-in-Chief, with the assistance of Yongjun Jiang, Associate Editor

Keywords:
Ecohydrology
Lorentzian spectrum
Mediterranean ecosystems
Root zone soil moisture

ABSTRACT

Storage of water within soil pores of the root zone introduce memory effects in the dynamics of soil moisture that are considerably longer than the integral timescale of many atmospheric processes. Thus, hydro-climatic states can be "sustained" through land-surface heat and water vapor fluxes primarily because they can "feed off" on this long-term soil moisture memory. Root-zone soil moisture memory is only but one feature characterizing the spectrum of soil moisture dynamics, which is analyzed here using a combination of long-term measurements and models. In particular, the spectrum of root-zone soil moisture content in a Mediterranean ecosystem is examined using 14-years of half-hourly measurements. A distinguishing hydro-climatic feature in such ecosystems is that sources (mainly rainfall) and sinks (mainly evapotranspiration) of soil moisture are roughly out of phase with each other. For over 4 decades of time scales and 7 decades of energy, the canonical shape of the measured soil moisture spectrum is shown to be approximately Lorentzian determined by the soil moisture variance and its memory but with two exceptions: the occurrences of a peak at diurnal-to-daily time scales and a weaker peak at near annual time scales. Model calculations and spectral analysis demonstrate that diurnal and seasonal variations in hydroclimate forcing responsible for variability in evapotranspiration had minor impact on the normalized shape of the soil moisture spectrum. However, their impact was captured by adjustments in the temporal variance. These findings indicate that precipitation and not evapotranspiration variability dominates the multi-scaling properties of soil moisture variability consistent with prior climate model simulations. Furthermore, the soil moisture memory inferred by the annual peak of soil moisture (340 d) is consistent with climate model simulations, while the memory evaluated from the loss function of a linearized mass balance approach leads to a smaller value (50 d), highlighting the effect of weak non-stationarity on soil moisture variability.

1. Introduction

While root-zone soil water is less than 0.001% of water on Earth (Shiklamonov, 1993), it affects a plethora of mass and energy exchange processes relevant to climate science, ecohydrology, crop production, and numerous ecosystem services (Seneviratne et al., 2010; Schwingshackl et al., 2017; Zhou et al., 2019). On short time scales (i.e.hourly to sub-daily), root-zone soil moisture content, hereafter labeled as θ, influences the partitioning of net radiation into latent (LE) and sensible (H) heat fluxes that, in turn, affect the dynamics of the atmospheric boundary layer depth (Shukla and Mintz, 1982; Koster et al., 2000; Siqueira et al., 2009; Koster et al., 2004; Seneviratne et al., 2010; van den Hurk et al., 2012; Schwingshackl et al., 2017; Haghighi et al., 2018; Ardilouze et al., 2020). On longer time scales (days to months), storage of water in the root-zone introduces memory that modifies hydro-climatic conditions impacting cloud formation and rainfall (P). Wet soil moisture states, when they persist for an extended period of time, can alter air relative humidity (to higher values) and vapor pressure deficit (to lower values) in the overlying atmosphere thereby altering the lifting condensation level, cloud formation, and rainfall. Thus wet soil moisture states that persist in time for an extended period (compared to hydro-climatic variability) allows atmospheric processes to 'feed off' this wet root-zone soil moisture state eliciting a positive feedback on the atmosphere - meaning pushing boundary layer processes towards preferential states that then favor rainfall thereby increasing the root-zone soil moisture. For these reasons, the investigation of θ variability at multiple time scales and its connection with atmospheric processes at different time scales is necessary for quantifying and modelling climatic, hydrological and ecological processes (Wang et al., 2006; Seneviratne et al., 2010). Several studies assessed the

* Corresponding author.
E-mail address: roberto.corona@unica.it (R. Corona).

https://doi.org/10.1016/j.jhydrol.2022.127757
Received 27 November 2021; Received in revised form 15 March 2022; Accepted 17 March 2022
Available online 24 March 2022

key role of the root-zone soil moisture variability on hydrological, ecological and climate models, and demonstrated how the model results are sensitive to the variability in the root-zone soil moisture content at different time-scales (Detto et al., 2006; Wang et al., 2006; Lozano-Parra et al., 2018; van Oorschot et al., 2021; Konings et al., 2021). The interactive effect between θ and P has been found to be stronger in areas where soil moisture temporal variability is enhanced such as in arid and semi-arid regions (Delworth and Manabe, 1988; Srivastava et al., 2021), and in transitional regions between dry and wet climate (Koster and Suarez, 1995; Seneviratne et al., 2010; McColl et al., 2017). For this reason, variability in θ at multiple time scales continues to draw attention in climate science and hydrology (Delworth and Manabe, 1988; Oglesby et al., 2002; Pan et al., 2001; Huang et al., 1996; Yeh et al., 1984; Mintz and Serafini, 1992; Dong et al., 2007; Albertson and Montaldo, 2003; Dirmeyer, 2011; Koster et al., 2004; Seneviratne et al., 2010; McColl et al., 2017) and frames the scope of the work here.

In practice, multi-scale variability in measured or modeled θ time series is quantified using the spectrum of soil moisture ($E_\theta(f)$) that satisfies the normalizing property

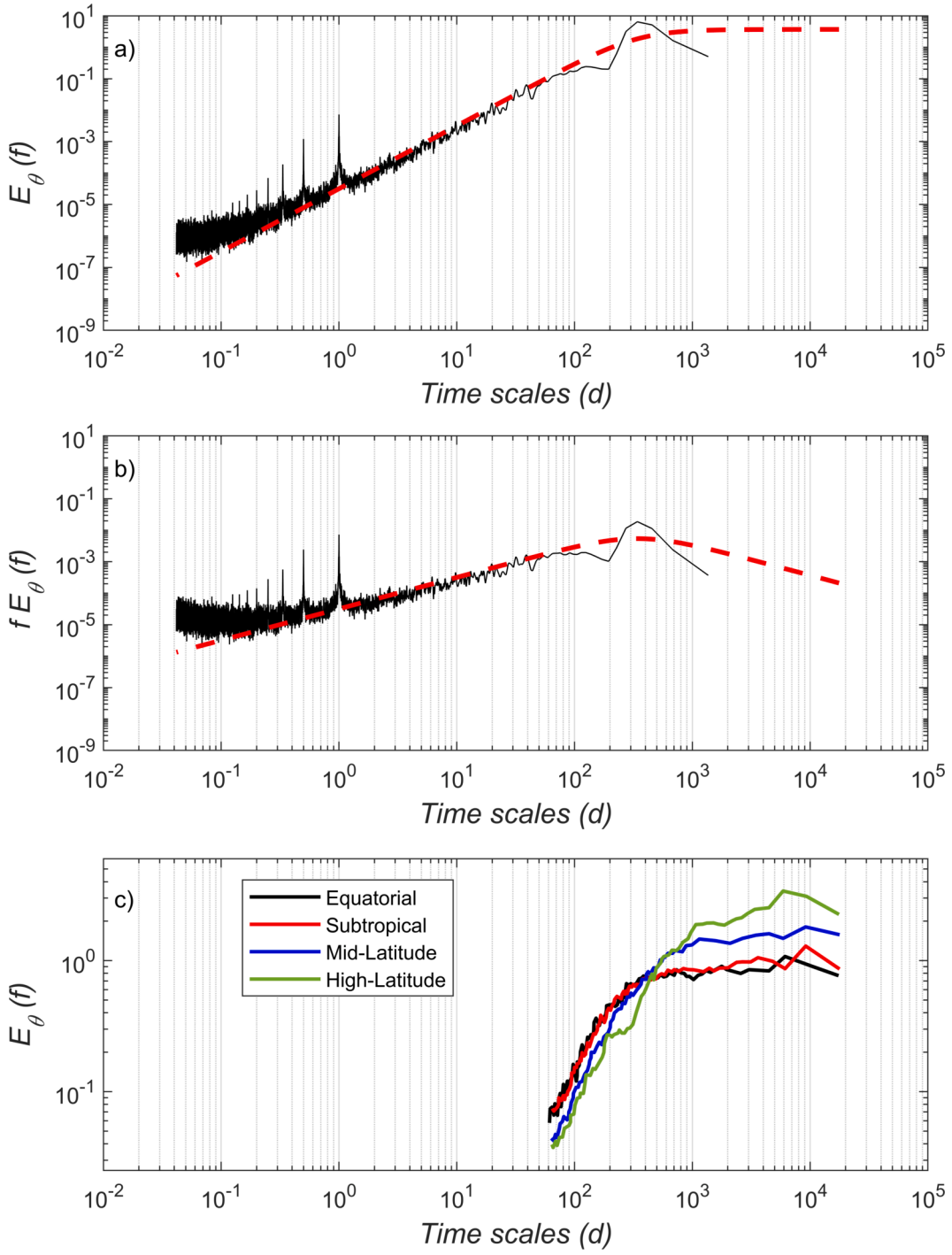

Fig. 1. Top panel: The measured Fourier $E_\theta(f)$ as a function of time scale or inverse frequency (i.e. f^{-1}), along with the Lorentzian curve (dashed red) at the Orroli site; Middle panel: measured pre-multiplied soil moisture Fourier spectrum $fE_\theta(f)$ as a function of time scale or inverse frequency (i.e. f^{-1}) along with the Lorentzian curve (dashed red) showing the peak at about 340 d; Bottom panel: the GCM derived $E_\theta(f)$ reported elsewhere (Delworth and Manabe, 1988) shown for reference.

$$\sigma_\theta^2 = \int_0^\infty E_\theta(f)df, \quad (1)$$

where f is the frequency (or inverse time scale) and σ_θ^2 is the temporal soil moisture variance. At the global scale, $E_\theta(f)$ was already derived from general circulation models (GCM) and often compared to a red noise process (i.e. $E_\theta(f) \sim f^{-2}$ (Delworth and Manabe, 1988; Nakai et al., 2014)). At much longer time scales, $E_\theta(f)$ is primarily forced by P and snow melt and dampened by evapotranspirational (ET) and drainage losses from the root zone. Under certain conditions such as white-noise spectrum for P and with ET losses scaling linearly with θ, $E_\theta(f)$ attains a 'Lorentzian' shape given by (Delworth and Manabe, 1988; Katul et al., 2007; Nakai et al., 2014; Ghannam et al., 2016)

$$E_\theta(f) = 2\sigma_\theta^2 \frac{\beta}{\pi} \frac{1}{\beta^2 + f^2}, \quad (2)$$

where β is related to the $1/e \approx 0.37$ folding time as well as soil moisture memory Γ, which is the time needed for a soil column to forget its wet conditions when induced by a rainfall event (Delworth and Manabe, 1988; Koster and Suarez, 1995; Ghannam et al., 2016). The Lorentzian spectrum converges to red noise when $f/\beta \gg 1$ and to white noise (i.e. $E_\theta(f) \sim f^0$) when $f/\beta \ll 1$ (Halley, 1996). At $f = \beta$, $fE_\theta(f)/\sigma_\theta^2 = 1/\pi$ as well as $d[fE(f)]/df = 0$ implying that $fE(f)$ is a maximum. For this reason, the so-called pre-multiplied spectrum $fE_\theta(f)$ can be used to operationally infer soil moisture memory from β. Viewed from this perspective, the "memory" timescale becomes a rough measure of the time needed by the root-zone soil column to "forget" an imposed anomaly such as a rainfall event (or lack thereof) as discussed elsewhere (Ghannam et al., 2016). Typical GCM derived $E_\theta(f)$ have been shown to follow a Lorentzian shape (see Fig. 1) but with decrease in β as latitude increases.

Moving beyond large-scale latitudinal variations, a number of studies have demonstrated that $E_\theta(f)$ is controlled by P and its seasonal dynamics, soil hydraulic properties, and vegetation cover (Koster and Suarez, 2001; Wei et al., 2006; Dong et al., 2007; Katul et al., 2007; Nakai et al., 2014; Ghannam et al., 2016). In general, $E_\theta(f)$ (or its Fourier pair, the autocovariance function) encodes the soil moisture memory Γ (Entin et al., 2000; Nakai et al., 2014; Ghannam et al., 2016). For a Lorentzian spectrum that is derived from a finite time series of θ, Γ may be determined empirically from the frequency at which $fE_\theta(f)$ attains its maximum (in this case $f = \beta$) as earlier noted. When drainage losses from the root-zone are small compared to the maximum ET (ET_{max}), an estimate of $\beta = ET_{max}/(\eta d_r)$ can also be derived (Katul et al., 2007; Nakai et al., 2014; Ghannam et al., 2016), where η is the soil porosity within the rooting zone and d_r is the root-zone depth. For an ET_{max}=5 mm d^{-1}, $d_r = 0.5$ m, and $\eta = 0.5$, the modeled $\Gamma \sim \beta^{-1} = 50$ d and is much longer than the time scales representing hydroclimatic variability (hours to few days). This long time scales (50 days) enables atmospheric processes to feed-off from persistent root-zone soil moisture states thereby experiencing an alteration in their own states through feedback mechanisms that are beginning to be uncovered (Delworth and Manabe, 1988; Vinnikov et al., 1996; Koster and Suarez, 2001; Seneviratne and Koster, 2012; Nicolai-Shaw et al., 2016; Ghannam et al., 2016). The memory of soil moisture, due to its connection with soil hydraulic properties (Martínez-Fernández et al., 2021; Katul et al., 2007), is spatially dependent and it is found to be higher in dry than wet areas (Katul et al., 2007; Ghannam et al., 2016; Martínez-Fernández et al., 2021). A number of other studies have also shown links between $E_\theta(f)$ and "persistence", which represents the probability that the soil moisture remains in a dry condition over a certain time period (Ghannam et al., 2016). For these reasons, the ability of climate and hydrological models to reproduce $E_\theta(f)$ across a wide range of f and across spatial scales is becoming a necessity (Pan et al., 1995; Delworth and Manabe, 1988; Huang et al., 1996; Yeh et al., 1984; Mintz, 1982; Dong et al., 2007; Koster et al., 2004; Seneviratne et al., 2010; Western et al., 2002; McColl et al., 2017; Zhu et al., 2020).

Some studies evaluated soil moisture variations produced by GCMs or regional land surface models using a network of extended in situ soil moisture observations (Guo and Dirmeyer, 2006; Xia et al., 2015; Yuan and Quiring, 2017; Knist et al., 2017). By and large, these studies conclude that soil moisture variability is reasonably represented by climate models when seasonal soil moisture patterns are adequately captured. However, large deviations between measured and modeled soil moisture was reported in transitional climatic areas (Yuan and Quiring, 2017; Knist et al., 2017). A case in point is the Mediterranean region where climatic and vegetation cover variations impact and are impacted by soil moisture (Knist et al., 2017; Quintana-Seguí et al., 2020). The Mediterranean region experiences high soil moisture variability and has been identified as a climatic area with strong coupling between the atmosphere and the land surface (Seneviratne et al., 2010; Knist et al., 2017; Hertig et al., 2019; Mimeau et al., 2021). Such strong coupling between soil moisture variability, vegetation cover changes (tree, grass, bare soil), and hydroclimatic conditions where P and air temperature (T_a) are seasonally out-of-phase with each other offers a dynamically interesting test case for assessing the controls on $E_\theta(f)$ and motivate the present work. The spectral properties of measured $E_\theta(f)$ sampled in a typical Mediterranean ecosystem and shown in Fig. 1 is considered. The main science question to be addressed is this: what hydroclimatic and hydrologic factors dictate the shape of $E_\theta(f)$? A particular focus is dedicated to the scaling laws of $E_\theta(f)$ with f, the dominant modes of variability, and Γ. More specifically, we seek to uncover signatures in $E_\theta(f)$ of key hydroclimatic factors and land surface cover transformation between tree/grass and tree/bare soil configurations. The data used to generate the spectrum in Fig. 1 were collected in Orroli, Sardinia where half-hourly measured soil moisture content, P,ET, and all the key terms in the energy balance have been collected for 14 years (starting in 2003) as described elsewhere (Montaldo et al., 2008; Montaldo et al., 2013; Montaldo et al., 2020). A land surface model (LSM) that accounts for dynamic vegetation through a biomass budget and all the hydrometeorological and energy balance considerations impacting the water budget is also employed to interpret mechanistically the measured $E_\theta(f)$ and the expected controls on it.

2. Materials and methods

2.1. Experimental site

The Orroli field site is a Mediterranean natural ecosystem located in east-central Sardinia (39°41' 12. 57" N, 9°16' 30. 34" E, 500 m a.s.l.; (Detto et al., 2006; Detto et al., 2008; Montaldo et al., 2008; Montaldo et al., 2013)). The climate is Maritime Mediterranean with mean annual P (1922–2017) of 643 mm but characterized by dry summers (11 mm in July). The mean annual air temperature (T_a) is 14.6 °C (mean T_a of 23.7 °C in July). The landscape is a mixture of woody vegetation and grass on a shallow (15–40 cm thick) silt loam soil (19% sand, 76% silt, 5% clay, bulk density of 1.38 g cm^{-3}, and η = 53%). The soil depth above a fractured rocky layer ranges between 10–50 cm, averaging 17 cm ± 6 cm (standard deviation, SD). The rooting depth d_r, for all practical purposes, is not constrained vertically by an optimizing between carbon investment below ground versus root-water (and nutrient) uptake. To the contrary, the entire soil above the fractured rock layer is populated by roots (grass, trees, or both). For this reason, the mean soil depth is assumed to represent the mean d_r. However, the presence of cracks, soil pockets with some water content were qualitatively estimated from observed electrical resistivity maps and shown to partially contribute to ET (Corona and Montaldo, 2020; Montaldo et al., 2020). More recently, the root-zone depth for grass and trees has been evaluated separately based on root observation trenches. Each trench was 7 m long and 0.2 m wide, extending to the underlying rock (Montaldo et al., 2021). The depth of the root-zone for the grass species was found to range from 1 cm to 20 cm but this depth is limited by the presence of fractured rock. The roots and their distribution is mainly horizontal in this zone. The root-

zone for trees is about 20 cm on average and again mostly limited by the fractured rock layer. Interestingly, some tree roots penetrating vertically into the fractured rock were also confirmed by these observation trenches (Montaldo et al., 2021).

The dominant wild olive trees are distributed in patches forming a canopy covering ~ 33% of the footprint area associated with the eddy-covariance flux measurements (~ 1.5 km^2). The surrounding inter-clump areas are covered by herbaceous and grass species during high moisture periods, becoming dry bare soil during the drier periods of summer as described elsewhere (Detto et al., 2006; Detto et al., 2008; Montaldo et al., 2008; Montaldo et al., 2013; Corona and Montaldo, 2020).

2.2. Soil moisture and micrometeorological measurements

Seven frequency domain reflectometer probes (FDR, Model CS-616, Campbell Scientific Instruments, Logan, Utah) were inserted in the soil close to the tower (3.3–5.5 m away) to measure soil moisture in the shallow root-zone layer. The CS-616 probes are 30 cm in length and can measure soil moisture when positioned at any probe orientation. The installation and calibration of the FDR sensors are detailed elsewhere (Montaldo et al., 2020; Montaldo et al., 2021) and are not repeated here. The presence of fractured rocks and reduced soil depth required the installation of most of the soil moisture sensors tilted from the sought vertical alignment. Soil moisture time series were then vertically averaged. After conducting a Fourier transformation on the soil moisture time series, the phase angle was computed and shown to be in-phase with precipitation time series on short time scales (or high frequency) but opposite at very long time scales (or low frequency) as discussed elsewhere (Katul et al., 2007).

We have also conducted a separate spectral analysis on the time series of soil moisture content for probes inserted in grass-dominated areas and probes under trees. The analysis revealed no appreciable differences in spectral shapes (Supplementary material Fig. S1). For this reason, we averaged all probes together and treated them as an ensemble-averaged time series in the ensuing analysis.

Meteorological measurements were made with conventional instruments installed on a 10 m tower since May 2003. A Licor-7500 CO2/H2O infrared gas analyzer (Licor, Lincoln, Nebraska) was used for measuring high frequency (10 Hz) CO_2 and H_2O concentration whereas a Campbell Scientific CSAT-3 sonic anemometer was used for measuring the 3-components of the velocity. These high frequency measurements were used to estimate half-hourly ET, H, and net ecosystem carbon dioxide exchange (NEE) using the eddy covariance method (Brutsaert, 2013; Garratt, 1992; Baldocchi, 2003). Measurements of incoming and outgoing short-wave and long-wave radiation were used to derive net radiation (R_n) and surface temperature (T_s). The T_a, air relative humidity, soil heat flux, and precipitation (P) were also measured at half-hourly time step. The complete list of variables, instruments and their heights, and data post-processing are described elsewhere (Montaldo et al., 2020). The fraction of vegetation cover and its distribution over the site was estimated from a multispectral high spatial resolution (2.8 m) satellite image (DigitalGlobe Inc.) based on a supervised classification scheme (Montaldo et al., 2008). Data analyzed here cover the period between 10 May 2003 and 3 August 2017.

2.3. Spectral analysis

In Fourier analysis, the determination of $E_\theta(f)$ from time series of soil moisture used the Welch averaged modified periodogram method. Here, the time series of spatially averaged soil moisture is first divided into 7 overlapping sections (in time), then a Hamming (or cosine) window is applied with zero-padding to enable the implementation of Fast-Fourier Transforms. Because of the presence of gaps and their potential impact on the scaling laws, an alternative spectral representation was also employed based on orthonormal wavelet transformation (OWT). For the wavelet spectra, the OWT coefficients were computed using a Fast Wavelet Transform algorithm utilizing a dyadic arrangement across scales. The Haar basis function was used to determine these wavelet coefficients in the wavelet half-plane as discussed elsewhere (Foufoula-Georgiou and Kumar, 1994; Kumar and Foufoula-Georgiou, 1993; Lee and Yamamoto, 1994; Katul et al., 2001; Stoy et al., 2005). The Haar wavelet was chosen because it is among the most localized basis functions in time (and thus optimal for detecting gaps in time series) but not in frequency (contrary to the Fourier basis). Thus, the Fourier and Haar OWT represent the two extremes of locality and continuity in the time–frequency domain. The OWT spectrum was computed at each dyadic scale by averaging the squared wavelet coefficients across time (Katul and Parlange, 1994). Due to the locality of the Haar wavelet in the time domain, the OWT spectrum was determined for a gap-filled and gap-infected time series with coefficients associated with gaps excluded when averaging the squared wavelet coefficients across scales. For ease of comparisons of spectra across different variables, all variables are first normalized to zero-mean and unit variance when assessing the effect of gaps in the time series.

2.4. The land surface model (LSM)

A land surface model (LSM) that has been calibrated and tested for the site (Montaldo et al., 2008) was used to estimate the dynamics of water and energy fluxes on a half-hour time step. Model evaluation and performance are discussed elsewhere (Montaldo and Oren, 2022), and the results of the statistical test of model performance are given in Table 3 in the aforementioned study. The model represents soil moisture from the root zone as a reservoir that supplies the bare-soil and vegetation. The root zone soil moisture also regulates the infiltration and runoff mechanisms. The root zone depth represents the lower boundary for the LSM, where the soil hydraulic properties dictate drainage losses. The surface temperature and the energy balance equations for sensible heat flux, ground heat flux, and the net radiation were all solved using an approach similar to the force-restore method (Noilhan and Planton, 1989). The hydraulic properties, including the soil water characteristic curve and hydraulic conductivity function, are specified for a silty soil using standard power-law relations with volumetric soil moisture (Clapp and Hornberger, 1978). The LSM is used for two purposes: (i) as a tool to define the factors that exert control on $E_\theta(f)$ above and beyond throughfall (I), and (ii) to 'gap-fill' ET and θ in the computations of $E_\theta(f)$ in the Fourier and wavelet domains. The model was also used in the OWT wavelet spectral comparisons between gap-infected and gap-filled θ series.

The LSM was run with five different configurations for which the seasonal and yearly variability of T_a, incoming shortwave radiation (R_{swin}), wind velocity (Wsp), leaf area index (LAI) for both vegetation species, and vapor pressure deficit (VPD) were individually arrested. These variables all impact ET, the primary loss term in the soil water hydrological balance. Each model configuration assumes a constant value for each of the aforementioned four variables: the value changes every year and set to the averaged mean value of the variable. The list of the five model configurations (hereafter indicated as C1, C2, C3, C4 and C5) are summarized below:

- C1-Constant mean air temperature
- C2-Constant incident shortwave radiation
- C3-Constant mean wind speed
- C4-Constant mean vapor pressure deficit
- C5-Constant leaf area index set to long-term mean value

2.5. A linearized model for $E_\theta(f)$

The five scenarios in the previous section are contrasted with a simplified hydrologic-only model predicting the shape of $E_\theta(f)$. In this simplified model, the soil water balance for the root zone is considered

and is given by

$$\frac{d\theta(t)}{dt} = \frac{1}{d_r}\left(I(t) - e_{bs} - e_g - e_{wv} - q_D\right), \quad (3)$$

where $I(t)$ is the throughfall rate infiltrating into the soil surface, e_{bs} is bare soil evaporation, e_g and e_{wv} are transpiration rates of grass and woody vegetation respectively, and q_D is the drainage flux set at d_r. Since q_D is small relative to the other hydrological fluxes, it is ignored when analyzing the controls on $E_\theta(f)$. Defining the overall loss as $L = a_1 e_{wv} + a_2 e_g + a_3 e_{bs}$ with $a_1 + a_2 + a_3 = 1, a_1, a_2$, and a_3 are the fraction of trees, grass, and bare soil cover, and upon naively assuming L scales linearly with θ, the simplified hydrological balance for the root-zone soil moisture can be expressed as

$$\eta d_r \frac{ds(t)}{dt} = I(t) - s(t)L_{max}, \quad (4)$$

where $s(t) = \theta(\eta d_r)^{-1}$ is the degree of saturation ($s(t) \in [0, 1]$). A model for $E_s(f)$ can now be analytically derived for this budget when multiplying Eq. (4) by e^{ift} (with $i^2 = -1$), integrating with respect to t to determine the Fourier coefficients of soil moisture in relation to the Fourier coefficients of throughfall, and then computing $E_s(f)$ from the squared Fourier amplitudes to yield

$$E_s(f) = \frac{E_{nI}(f)}{\beta_L^2 + f^2}, \quad (5)$$

where $E_{nI}(f)$ is the spectrum of normalized throughfall $I(t)(\eta d_r)^{-1}$ that is related but not identical to rainfall (due to variations in LAI) and need not be white noise, $\beta_L = L_{max}(\eta d_r)^{-1}$ is the inverse of memory, and $f \in [0, \infty]$. The throughfall rates infiltrating into the soil covered by vegetation is modeled through a balance equation of the intercepted water by the canopy reservoir (its capacity is a function of the LAI), which produces throughfall when the reservoir is saturated, as described elsewhere (Noilhan and Planton, 1989). This spectrum is considered as a 'reference' given that the variability in hydrometeorological drivers and vegetation dynamics considered in *C*1–*C*5 are non-existent in this formulation. The only external driver affecting the soil moisture spectrum in Eq. (5) is temporal variability in I. Thus, this spectrum is contrasted with the spectrum derived from the calibrated LSM approach as well as those computed from cases *C*1–*C*5 applied to the LSM that capture all the complex time-dependent interactions between hydroclimatic variables, dynamic vegetation, and non-linear relation between losses from the root-zone and soil moisture.

2.6. Data gap filling

The soil moisture long-term dataset invariably includes gaps resulting from electrical power loss or instrument failure. Gaps were more frequent during winter (≈ 18% of total) because reduced incoming solar radiation limited the recharge of batteries that power the entire system. Missing data of P were replaced with observations from a nearby rain-gauge station in Nurri (located 4 km from the Orroli site). Missing T_a and other hydroclimatic variables were replaced with measurements from a nearby weather station in Mandas (≈ 10 km from the Orroli site) (Montaldo et al., 2021). Gaps in θ and ET were replaced with a corresponding land-surface model (LSM) predictions calibrated for the site and later described. Spectral analysis was conducted in Fourier (local in frequency but not in time) and Haar wavelet domains. As noted earlier, the former is much better suited for detecting precise frequencies where $E_\theta(f)$ may be large whereas the latter is better suited for a 'gap-infected' time series characterized by pulses (Katul et al., 2001; Stoy et al., 2005). A preliminary analysis demonstrated that the OWT spectra of hydrometeorological variables including gaps and gap-filled series did not show significant differences at all time scales considered.

3. Results

Fig. 1c repeats prior GCM derived $E_\theta(f)$ (Delworth and Manabe, 1988) for four different latitudinal bands (Equatorial, Subtropical, Mid-Latitude, and High-Latitude). There is a clear increase in redness in the GCM derived $E_\theta(f)$ with the increase in latitude. The frequency where $E_\theta(f)$ transitions from 'white' to a finite exponent also shifts when moving towards the highest latitudes (time scales of ≈ 200 d for Equatorial and Subtropical, and ≈ 780 d for Mid-Latitude and High-Latitude bands). For the Mediterranean region studied here, the $E_\theta(f)$ is computed at higher temporal resolution and exhibit clear peaks at daily, sub-daily and annual time scale (≈ 341 d) as shown in Fig. 1a. At frequencies exceeding 100 days (not resolved in the GCM derived $E_\theta(f)$), $E_\theta(f)$ exhibits an approximate power-law (i.e. $E_\theta(f) \sim f^\alpha$ with an exponent close to $\alpha = -2$). Near the sampling frequency range (or time scales < 0.1 d), the measured spectrum resembles white-noise likely due to random errors in FDR soil moisture measurements (including electronics, detection of reflected energy content, etc.). The FDR can measure soil moisture at higher sampling frequencies when compared to time domain reflectometry but the signal to noise ratio is lower. The spectrum of measured soil moisture is also compared with the Lorentzian shape predicted from Eq. (2), with β determined empirically from the frequency at which $fE_\theta(f)$ (Fig. 1b) reaches its maximum (1/f = $1/\beta$ = 341 d). The main features of the measured soil moisture spectrum are reasonably described by such Lorentzian shape (but not the peaks at diurnal-to-daily and near-annual). For the low frequencies $E_\theta(f)$, some deviations from constant (white-noise) are expected due to the seasonality of $I(t)$ common to Mediterranean climates. However, the record here is not sufficiently long to ascertain the precise spectral shape at decadal time scales (though the GCM runs suggest near-white spectra at time scales exceeding 10^4 d for all regions). Nonetheless, the measured spectral peak here appear to be in line with GCM runs: it is longer than equatorial and sub-tropical regions but shorter than mid and high latitude regions reported in Fig. 1c.

Returning to the hydro-climate forcing, the monthly incident shortwave radiation and mean air temperature show the same pattern (i.e. they are in phase). The highest monthly values occur during the summer months (Fig. 2a and b). Precipitation and soil moisture time series are roughly in phase with each other but out of phase with incident shortwave radiation and air temperature. The lowest P and θ occur during the driest months of the year (June, July and August) (Fig. 2c and d). The decrease in θ begins in the month of May due to the increase in air temperature along with ET (Fig. 2f), and reduced P. Soil moisture increases again in September, with the increasing frequency of precipitation events. The VPD is in phase with P and θ (Fig. 2e), and it is for this reason that its variability is highest during the summer when both precipitation and soil moisture are low. Interestingly, monthly variations of ET, which is the main loss from the rooting zone in the hydrological balance, is not precisely in phase (or out of phase) with any of the hydro-climatic drivers or soil moisture in Fig. 2f. This finding confirms the role of land-cover switches on ET variability, but as shown later, less so on the normalized spectrum of θ. The normalized spectra of VPD, ET, θ, and the meteorological variables (R_{swin}, T_a, P) in Fig. 3 have been estimated for the gap-infected (top) and gap-removed (middle) time series using the orthonormal wavelet transform (Fig. 3a and Fig. 3b, respectively), and applying the Fourier analyses for the gap-removed time series (Fig. 3c). The normalized Haar wavelet power spectra of θ, the meteorological variables (R_{swin}, T_a, P), and ET show the same pattern except for P and θ for both the gap-infected (Fig. 3c) and the gap-removed time series (Fig. 3b). No significance difference were found comparing the spectra in Fig. 3a and Fig. 3b. While the energy distribution among time scales is most distributed for P when compared to other hydro-climatic variables, P is clearly not a white noise process. The meteorological variables and ET, all exhibit common features for the time occurrence of spectral peaks, which are localized at daily and annual time scales. There is a difference in the power magnitude at daily

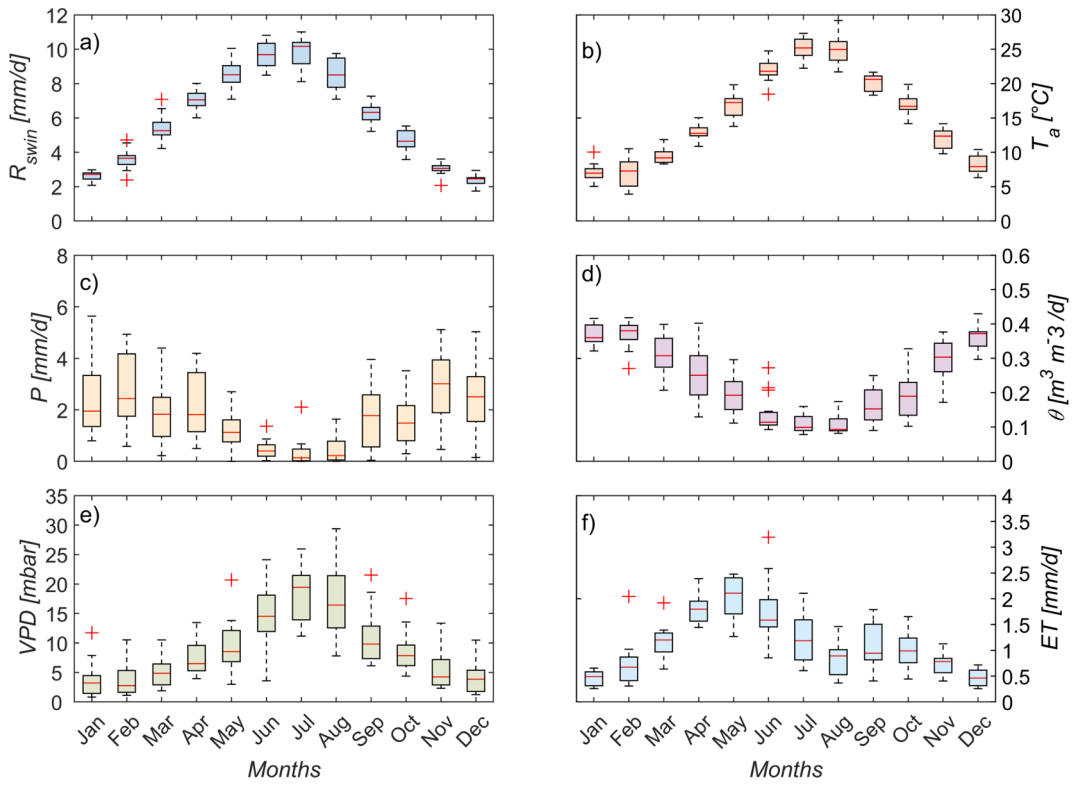

Fig. 2. Ensemble monthly variations for the period 2003–2017 of observed (a) incoming shortwave solar radiation (R_{swin}), (b) air temperature (T_a), (c) precipitation (P), (d) soil moisture content (θ), (e) vapor pressure deficit (VPD), and f) evapotranspiration (ET). Boxplots show the median (red horizontal line), 25th and 75th percentiles (top and bottom of the shaded box, respectively), and maximum and minimum observed values (edges of the top and bottom whiskers, respectively).

time scales, where *Rswin* and *ET* are three order of magnitude higher than the θ spectrum, and almost one order of magnitude higher than T_a, P and VPD spectrum (Fig. 3b). Considering that the OWT spectra of hydrometeorological variables for gap-removed series did not significantly differ from gap-infected spectra (Fig. 3a and Fig. 3b, respectively), the gap-removed series are used with the Fourier approach (Fig. 3c) given its superior localization in the frequency domain. Even if the Fourier approach detects the spectral variability of all hydrometeorological variables better than the OWT, the differences with the OWT spectra in Fig. 3b are not as relevant to the spectral exponents. The spectra of θ for both Fourier and OWT methodologies for gap-removed time series (violet line and thick black line, respectively, Fig. 3d), show some reduced variance compared with the spectra for gap-infected time series (thick red line, Fig. 3d), but the overall shape is not modified.

The soil moisture time series estimated with the five runs of the LSM allowed evaluating the effect of censoring the seasonal and yearly variability of $T_a, R_{swin}, W_{sp}, VPD$ and LAI, (C1, C2, C3, C4, C5 configurations, respectively) on the modeled normalized soil moisture spectra $E_{\theta m}(f)$, (Fig. 4a and Fig. 4b). For each model configuration, the OWT normalized spectra of $E_\theta(f)$ does not show any significant difference with that of the calibrated LSM that includes all the hydrometeorological variability (Fig. 4a). The estimated $E_{\theta m}(f)$ with Fourier analysis shows the same behaviour for all the model configurations, with peaks localized at the seasonal, daily and sub daily time scales, as was in OWT analysis. Nevertheless, the modeled soil moisture time series are different from each other (Supplementary material Fig. S2a). However, this difference, to a leading order, is not in the shape of the spectrum but in the area under the actual spectrum (i.e. the soil moisture variance). The normalized relative differences between the variances of the $E_{\theta m}(f)$ estimated with the calibrated model and obtained for C1 and C5 configurations is about −11 % and 7 %, respectively (Supplementary material Fig. S2b).

At high frequencies, the behaviour of normalized $E_\theta(f)$ is the same for all model configurations suggesting the absence of any appreciable hydrometeorological and vegetation dynamic effect on the soil moisture spectrum (Fig. 4a and Fig. 4b) beyond I. This finding is in line with E_θ being controlled by variability in P and soil moisture memory instead of the hydrometeorological controls on ET. The normalized spectra of P and *modeled* I from P and LAI unsurprisingly have the same behaviour (Fig. 4c) and show a spectral decay reasonably described by a power-law (i.e. $E_P(f) \sim f^\alpha$. The exponent $\alpha = -0.3$ at 1 to 10-day time scales but increases to $\alpha = -0.75$ at sub-daily (or storm) time scale. For convective storms, $\alpha = -1$ whereas for frontal systems, $\alpha = -0.5$ (Molini et al., 2009). Hence, an $\alpha = -0.75$ at sub-daily time scales here resides in-between these two storm types. The normalized spectrum of soil moisture content $E_s(f)$ given by the linear model of Eq. (5) is compared with the measured spectrum of θ estimate with the OWT and Fourier approaches in Fig. 5a and in Fig. 5b, respectively. The linear model predicts a spectral decay of θ that is characterized by two scaling regimes $E_s(f) \sim f^\alpha$ as expected: the exponent α is equal to −2.3 at 1 to 10-day time scales, while it is $\alpha = -2.75$ for the lowest frequencies. However, measured $E_\theta(f)$ appears to be described by a single power-law with $\alpha = -2$ for all the frequencies between 1 and 10 days, and differently than the linear model it shows peaks at daily, sub-daily and seasonal time scales. The OWT transform limits the presence of noise at the high frequency and its shape is also well represented by a single power-law (i.e. $E_P(f) \sim f^\alpha$ with $\alpha = -2$ Fig. 5a), than what is obtained with the Fourier methodology (Fig. 5b). The OWT cannot resolve energy at precise frequencies (e.g. diurnal and daily time scales) because of the dyadic arrangement in scale decomposition and its non-locality in the frequency domain. These are some the reasons why the OWT spectrum reveals a single $\alpha = -2$ for the soil moisture spectrum without 'bumps' on diurnal and daily time scales.

To be clear, differences in the normalized spectral estimates between Fourier and Haar based OWT methods (including scaling exponents) are to be expected. The two approaches decompose the time series using

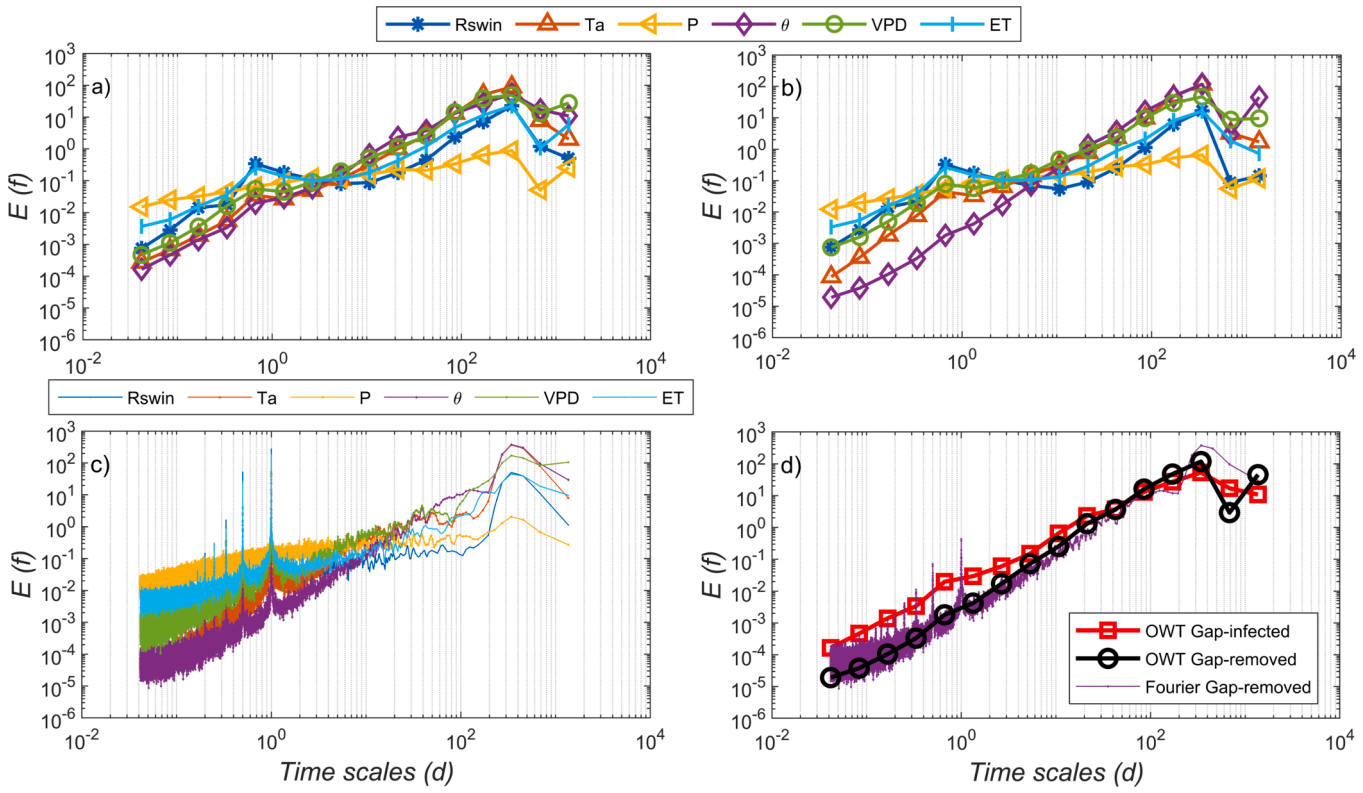

Fig. 3. Panel a: The normalized OWT power spectra of incoming shortwave solar radiation (*Rswin*), mean air temperature (T_a), precipitation (*P*), soil moisture content (θ), vapor pressure deficit (*VPD*), and evapotranspiration (*ET*) determined for gap-infected series. Panel b: Same as panel a but for gap-removed time series. Panel c: the Fourier power spectra for the gap-removed time series shown for comparison with panel b. Panel d: Comparison between OWT soil moisture spectra for gap-infected (red-square) and gap-removed (black open circles) time series along with the Fourier power spectrum for the gap removed time series repeated for reference. The time series of all variables are normalized to zero-mean and unit variance prior to spectral analyses to permit comparisons.

different basis functions and processing algorithms (e.g. boundary conditions at edges, tapering and windowing, dyadic arrangements, etc…). For finite and multi-scaled time series (such as the ones analyzed here), we wish to emphasize that there is no "correct" or "true" spectrum and the only necessary condition for the scale-wise decomposition (Fourier or Haar based OWT) is conservation of spectral energy when summed across all frequencies. Both transformations (Fourier and Haar-based OWT) satisfy this condition (i.e. Parseval's identity).

4. Discussion and conclusions

The connection between the soil moisture state and atmospheric processes at different scales has made the investigation of θ variability a necessity for quantifying and modelling climatic, hydrological and ecological processes. In this study, a 14-year soil moisture time series record collected at a Mediterranean site provided an opportunity to investigate variability in soil moisture at multiple time scales ranging from hours to more than a decade. A unique feature of this data set is that measured precipitation (main source of soil moisture) and eddy-covariance measured *ET* (main sink of soil moisture) are roughly (but not precisely) out of phase with each other. The spectrum of measured θ evaluated with Fourier analysis showed spectral peaks at diurnal-to-daily and close to annual time scales (≈ 341 *d*). Beyond those peaks, $E_\theta(f)$ attains a near-Lorentzian shape analogous to what was computed by GCMs (Fig. 2c) (Delworth and Manabe, 1988; Katul et al., 2007; Nakai et al., 2014; Ghannam et al., 2016) but with some differences. Unlike the GCM spectra, the measured spectrum of θ here does not attain a well-defined constant value independent of frequency at low frequencies (>1 year), though longer records are needed to reliably resolve this issue. That the measured soil moisture spectrum appears reasonably approximated by a near-Lorentzian shape perturbed by two well-defined peaks may lead to the conclusion that a linearized mass balance analysis driven by rainfall-only suffices to explain the key drivers of $E_\theta(f)$. Partial support for this conclusion stems from the fact that variability in the key hydrometeorological variables (Fig. 2) had minor impact on the shape of the normalized θ variability and rainfall variability remains the most influential factor explaining the shape of the normalized soil moisture spectrum (Koster and Suarez, 2001; Wei et al., 2006; Dong et al., 2007; Katul et al., 2007; Nakai et al., 2014). Indeed, the use of a linear model for $E_\theta(f)$ (i.e. Eq. (5)) where the variability of external drivers are not included but only the spectrum of modeled throughfall is used recovers both - the overall features of the measured spectrum of soil moisture as well as those obtained from a detailed land-surface formulation that accommodates variability in hydrometeorological drivers and land cover type. However, this conclusion is premature and naive on 2 accounts.

The memory inferred from the measured peak of the pre-multiplied Lorentzian spectrum (340 d) appears commensurate with expected interpolated values from GCMs for such a Mediterranean climate. The memory inferred from the loss function of the linearized mass balance approach (leading to a Lorentzian spectrum) where eddy-covariance measured *ET* and root-zone depth are used lead to a much smaller value (50 d). This finding points to the fact that weak non-stationarity or low-frequency modes introduce appreciable shifts in soil memory (by a factor of 7 here).

Moreover, the scaling laws at high frequency do not strictly abide by predictions from the linearized mass balance analysis. At sub-daily time scale, the spectrum of rainfall exhibits a scaling law commensurate with $f^{-0.75}$. Hence, the linearized mass balance analysis predicts that the spectrum of soil moisture scales as $f^{-2.75}$. The exponent estimate here from the measured soil moisture spectrum remains consistent with an f^{-2}. Moving to time scales commensurate with 10 days, the precipitation

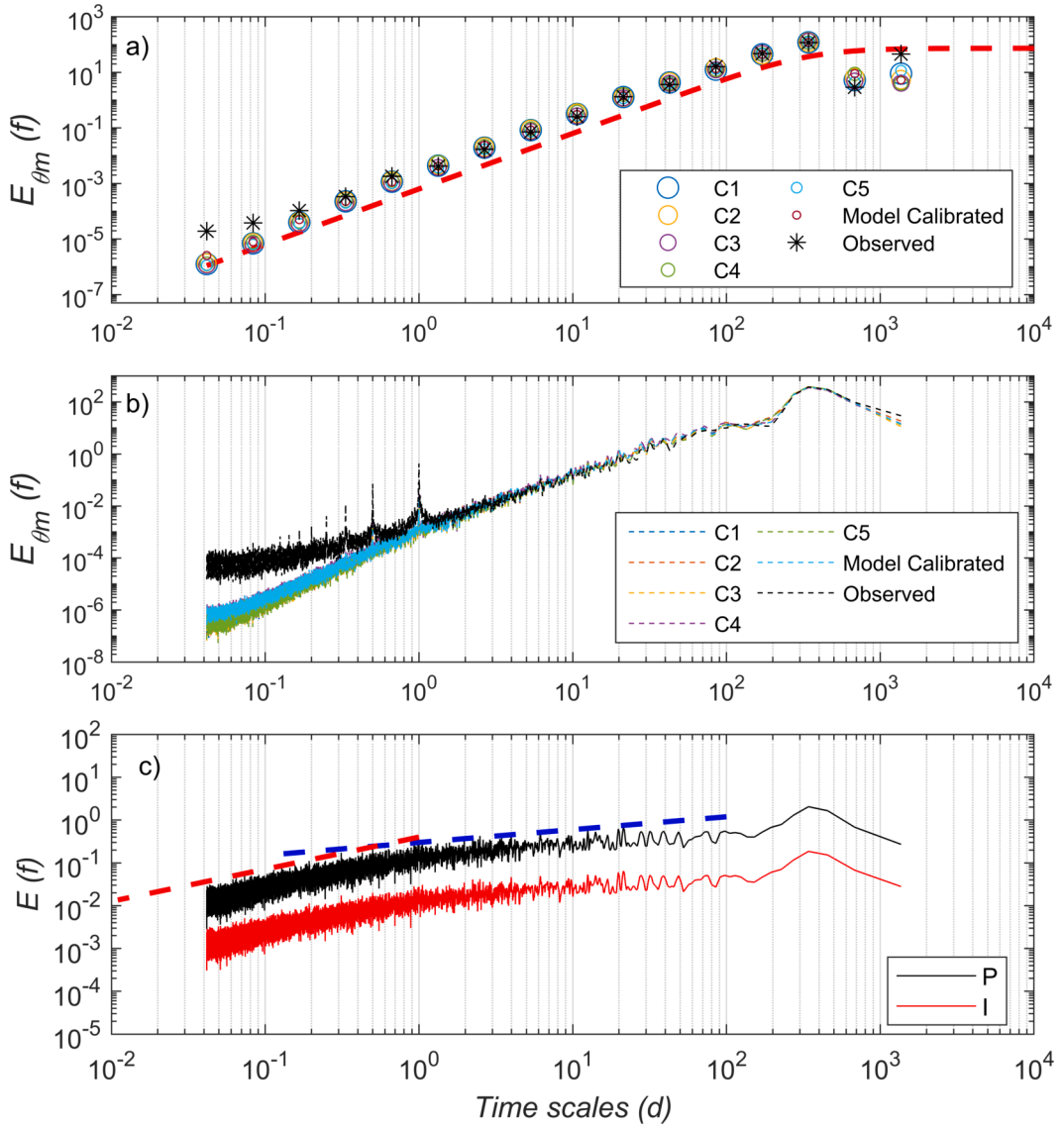

Fig. 4. Top panel: The OWT normalized power spectrum of modeled soil moisture $E_{\theta_m}(f)$ evaluated for configurations C1 (constant air temperature), C2 (constant incoming solar radiation), C3 (constant wind velocity), C4 (constant vapor pressure deficit), C5 (constant LAI), and the full LSM scheme (open circle) as a function of time scale or inverse frequency. The Lorentzian spectrum (red-dashed) and the OWT spectrum derived from measured soil moisture are repeated for reference. Middle panel: Same as above but for the Fourier domain. Bottom panel: the normalized Fourier power spectrum of observed precipitation (P) and modeled throughfall rate infiltrating into the soil (I) derived from P and LAI: the blue and red dashed lines are the fitted scaling laws: $f^{-0.3}$ and $f^{-0.75}$, respectively. The spectra of P and I are offset by one decade in the vertical for clarity.

spectrum scales as $f^{-0.3}$ and thus the predicted soil moisture spectral scaling exponent from linearized mass balance analysis is $f^{-2.3}$. Once again, the measured soil moisture spectrum maintains its approximate f^{-2} range for those time scales.

These deviations between measured and modeled soil moisture Fourier spectra suggest that during summer months, trees may be withdrawing water from much deeper layers - and this withdrawal generates an effective root-zone depth that can exceed the assumed root-zone depth here (constrained by soil depth above the fractured rock layer). An increase in the effective root-zone depth increases the memory predicted from the linearized mass balance ($\Gamma = \eta d_r / ET_{max}$). There is already partial evidence that trees are withdrawing water from well below the assumed rooting zone during summer months as noted earlier here and in prior studies (Corona and Montaldo, 2020; Montaldo et al., 2021). This analysis ignores the more significant effect that such a withdrawal can also be non-stationary (i.e. d_r fluctuates at low frequency). Whether the non-stationarity in d_r alone is sufficient to shift the soil moisture memory by a factor of 7 alone remains unclear and requires targeted experiments. Hence, differences in the two soil moisture memory estimates here (peak in the spectrum and $\Gamma = \eta d_r / ET_{max}$) point to an under-appreciated role of a vertically dynamic root water extraction.

In addition, we speculate that the relation between measured rainfall and measured increases in spatially-averaged stored water during rainfall is noisy (Supplementary Fig. S3a and b) pointing to some 'randomization' effect (in both time and space). If so, this randomization implies that short-term correlations in rainfall (described by the rainfall spectral exponent) are partially destroyed by throughfall and subsequent infiltration process as detected by increases in stored water in individual FDR probes during rainfall. This conjectured randomization may explain why the measured soil moisture spectral exponent remains close to f^{-2} (red noise) and not $f^{-2.3}$ to $f^{-2.8}$ (black noise) as predicted from the Fourier transformed linear hydrological balance at short to intermediate time scales (at least for the probe locations analyzed here).

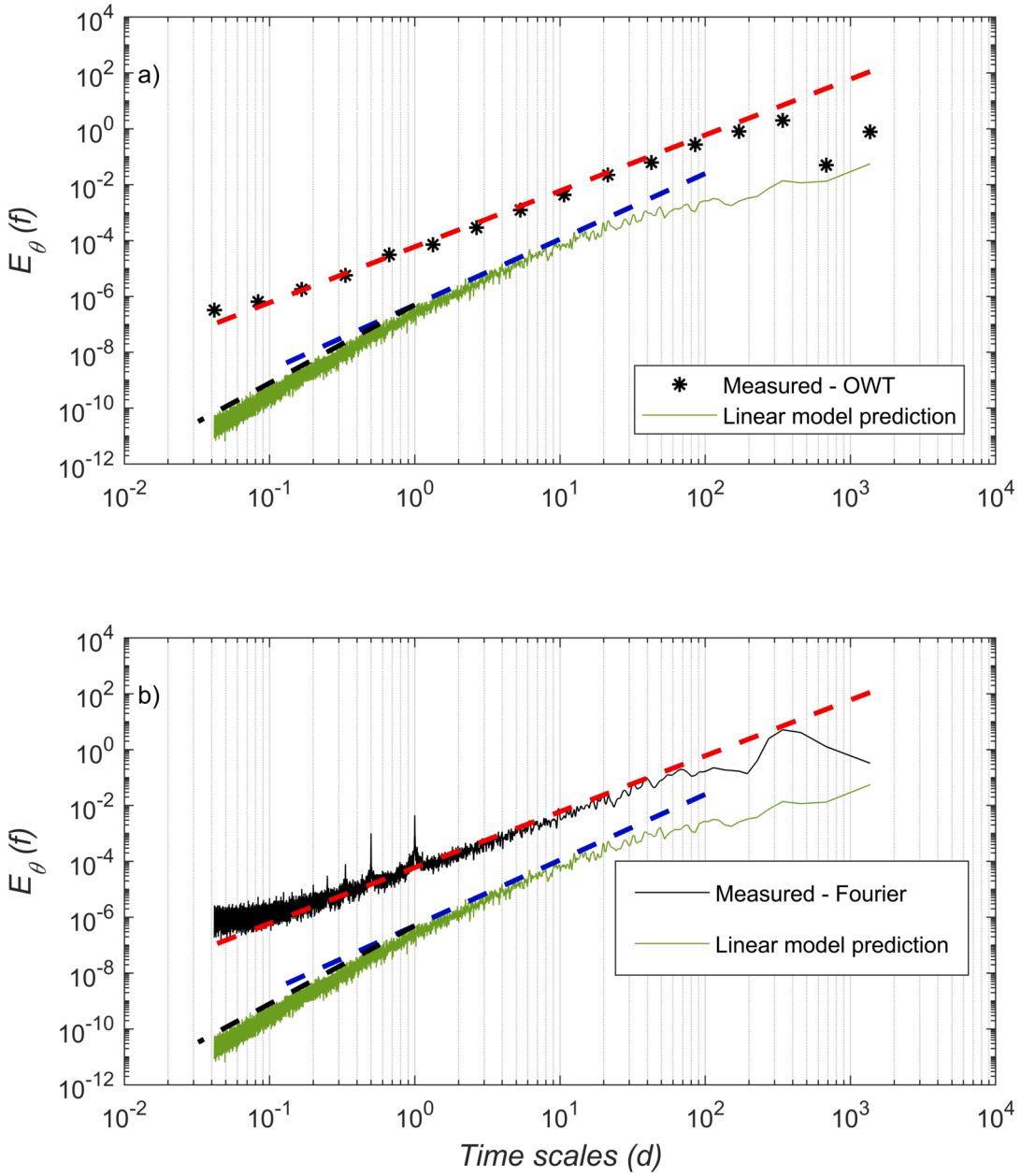

Fig. 5. Top panel: The normalized spectrum of soil moisture estimated with the linearized hydrological balance model $E_s(f)$ from Eq. (5) compared with the measured spectrum of soil moisture $E_\theta(f)$ (shown for the OWT). Bottom panel: the same but in the Fourier domain. The red dashed line is the f^{-2} scaling (or the red-noise spectrum), while the blue and black dashed lines are $f^{-2.35}$ and $f^{-2.8}$, respectively. The spectra of the observed and modeled are offset by three decades in the vertical for clarity.

Again, the role of throughfall appears to play a role in shaping the normalized soil moisture spectral exponent from sub-daily to monthly time scales.

Not withstanding these issues, it is clear that deviations between measured and modeled spectra offer a new perspective about two eco-hydrological processes. Specifically, intermittent extraction of water by deep roots (i.e. memory deviations on long time scales) and the role of randomness in infiltration destroying rainfall memory within the root-zone at short to intermediate time scales warrant directed explorations in the future.

Declaration of Competing Interest

The authors declare that they have no known competing financial interests or personal relationships that could have appeared to influence the work reported in this paper.

Acknowledgments

RC and NM acknowledge support by the Ministry of Education, University and Research (MIUR) through the ALTOS European project of PRIMA MED, CUP n. F24D19000020006, the SWATCH European project of the PRIMA MED program, CUP n. F24D19000010006, and the FLUXMED European project of the WATER JPI program, CUP n. F24D19000030001. GK acknowledges support from the U.S. National Science Foundation (NSF-AGS-2028633, NSF-IOS-1754893), and the Department of Energy (DE-SC0022072). We also acknowledge Riccardo Piras for his support in data analysis. Finally we thank the Meteoclimatic Department of ARPA Sardegna for providing the meteorological data and the Sardinian water authority (ENAS) for supporting the eddy

covariance tower installation and maintenance.

Appendix A. Supplementary data

Supplementary data associated with this article can be found, in the online version, at https://doi.org/10.1016/j.jhydrol.2022.127757.

References

Albertson, J.D., Montaldo, N., 2003. Temporal dynamics of soil moisture variability: 1. Theoretical basis. Water Resour. Res. 39 (10) https://doi.org/10.1029/2002WR001616.

Ardilouze, C., Materia, S., Batté, L., Benassi, M., Prodhomme, C., 2020. Precipitation response to extreme soil moisture conditions over the Mediterranean. Clim. Dyn. 1–16.

Baldocchi, D.D., 2003. Assessing the eddy covariance technique for evaluating carbon dioxide exchange rates of ecosystems: past, present and future. Glob. Change Biol. 9 (4), 479–492.

Brutsaert, W., 2013. Evaporation into the Atmosphere: Theory, History and Applications, 1. Springer Science & Business Media.

Clapp, R.B., Hornberger, G.M., 1978. Empirical equations for some soil hydraulic properties. Water Resour. Res. 14 (4), 601–604.

Corona, R., Montaldo, N., 2020. On the transpiration of wild olives under water-limited conditions in a heterogeneous ecosystem with shallow soil over fractured rock. J. Hydrol. Hydromech. 68 (4), 338–350.

Delworth, T., Manabe, S., 1988. The influence of potential evaporation on the variabilities of simulated soil wetness and climate. J. Clim. 1, 523–547.

Detto, M., Montaldo, N., Albertson, J.D., Mancini, M., Katul, G., 2006. Soil moisture and vegetation controls on evapotranspiration in a heterogeneous Mediterranean ecosystem in Sardinia, Italy. Water Resour. Res. 42 (8) https://doi.org/10.1029/2005WR004693.

Detto, M., Katul, G., Mancini, M., Montaldo, N., Albertson, J., 2008. Surface heterogeneity and its signature in higher-order scalar similarity relationships. Agric. For. Meteorol. 148 (6–7), 902–916.

Dirmeyer, P.A., 2011. The terrestrial segment of soil moisture–climate coupling. Geophys. Res. Lett. 38 (16) https://doi.org/10.1029/2011GL048268.

Dong, J., Ni-Meister, W., Houser, P.R., 2007. Impacts of vegetation and cold season processes on soil moisture and climate relationships over Eurasia. J. Geophys. Res.: Atmos. 112 (D9) https://doi.org/10.1029/2006JD007774.

Entin, J.K., Robock, A., Vinnikov, K.Y., Hollinger, S.E., Liu, S., Namkhai, A., 2000. Temporal and spatial scales of observed soil moisture variations in the extratropics. J. Geophys. Res.: Atmos. 105 (D9), 11865–11877.

Foufoula-Georgiou, E., Kumar, P., 1994. Wavelet Analysis in Geophysics: An Introduction, 4. Elsevier.

Garratt, J., 1992. The Atmospheric Boundary Layer. Cambridge University Press.

Ghannam, K., Nakai, T., Paschalis, A., Oishi, C.A., Kotani, A., Igarashi, Y., Kumagai, T., Katul, G.G., 2016. Persistence and memory timescales in root-zone soil moisture dynamics. Water Resour. Res. 52 (2), 1427–1445.

Guo, Z., Dirmeyer, P.A., 2006. Evaluation of GSWP-2 soil moisture simulations, Part I: inter-model comparison. Journal of Geophysical Research 111, D22S02.

Haghighi, E., Short Gianotti, D.J., Akbar, R., Salvucci, G.D., Entekhabi, D., 2018. Soil and atmospheric controls on the land surface energy balance: a generalized framework for distinguishing moisture-limited and energy-limited evaporation regimes. Water Resour. Res. 54 (3), 1831–1851.

Halley, J.M., 1996. Ecology, evolution and 1/f-noise. Trends Ecol. Evol. 11 (1), 33–37.

Hertig, E., Tramblay, Y., Romberg, K., Kaspar-Ott, I., Merkenschlager, C., 2019. The impact of soil moisture on precipitation downscaling in the Euro-Mediterranean area. Clim. Dyn. 52 (5), 2869–2884.

Huang, J., van den Dool, H.M., Georgarakos, K.P., 1996. Analysis of model-calculated soil moisture over the United States (1931–1993) and applications to long-range temperature forecasts. J. Clim. 9 (6), 1350–1362.

Katul, G.G., Parlange, M.B., 1994. On the active role of temperature in surface-layer turbulence. J. Atmos. Sci. 51 (15), 2181–2195.

Katul, G., Lai, C.-T., Schäfer, K., Vidakovic, B., Albertson, J., Ellsworth, D., Oren, R., 2001. Multiscale analysis of vegetation surface fluxes: from seconds to years. Adv. Water Resour. 24 (9–10), 1119–1132.

Katul, G.G., Porporato, A., Daly, E., Oishi, A.C., Kim, H.-S., Stoy, P.C., Juang, J.-Y., Siqueira, M.B., 2007. On the spectrum of soil moisture from hourly to interannual scales. Water Resour. Res. 43 (5) https://doi.org/10.1029/2006WR005356.

Knist, S., Goergen, K., Buonomo, E., Christensen, O.B., Colette, A., Cardoso, R.M., Fealy, R., Fernández, J., García-Díez, M., Jacob, D., et al., 2017. Land-atmosphere coupling in EURO-CORDEX evaluation experiments. J. Geophys. Res.: Atmos. 122 (1), 79–103.

Konings, A.G., Saatchi, S.S., Frankenberg, C., Keller, M., Leshyk, V., Anderegg, W.R., Humphrey, V., Matheny, A.M., Trugman, A., Sack, L., et al., 2021. Detecting forest response to droughts with global observations of vegetation water content. Global Change Biol. 27 (23), 6005–6024.

Koster, R.D., Suarez, M.J., 1995. Relative contributions of land and ocean processes to precipitation variability. J. Geophys. Res.: Atmos. 100 (D7), 13775–13790.

Koster, R.D., Suarez, M.J., 2001. Soil moisture memory in climate models. J. Hydrometeorol. 2 (6), 558–570.

Koster, R.D., Suarez, M.J., Heiser, M., 2000. Variance and predictability of precipitation at seasonal-to-interannual timescales. J. Hydrometeorol. 1 (1), 26–46.

Koster, R.D., Dirmeyer, P.A., Guo, Z., Bonan, G., Chan, E., Cox, P., Gordon, C., Kanae, S., Kowalczyk, E., Lawrence, D., et al., 2004. Regions of strong coupling between soil moisture and precipitation. Science 305 (5687), 1138–1140.

Kumar, P., Foufoula-Georgiou, E., 1993. A multicomponent decomposition of spatial rainfall fields: 2. Self-similarity in fluctuations. Water Resour. Res. 29 (8), 2533–2544.

Lee, D.T., Yamamoto, A., 1994. Wavelet analysis: theory and applications. Hewlett Packard J. 45, 44.

Lozano-Parra, J., Pulido, M., Lozano-Fondón, C., Schnabel, S., 2018. How do soil moisture and vegetation covers influence soil temperature in drylands of Mediterranean regions? Water 10, 1747.

Martínez-Fernández, J., González-Zamora, A., Almendra-Martín, L., 2021. Soil moisture memory and soil properties: an analysis with the stored precipitation fraction. J. Hydrol. 593, 125622.

McColl, K.A., Alemohammad, S.H., Akbar, R., Konings, A.G., Yueh, S., Entekhabi, D., 2017. The global distribution and dynamics of surface soil moisture. Nat. Geosci. 10 (2), 100–104.

Mimeau, L., Tramblay, Y., Brocca, L., Massari, C., Camici, S., Finaud-Guyot, P., 2021. Modeling the response of soil moisture to climate variability in the Mediterranean region. Hydrol. Earth Syst. Sci. 25 (2), 653–669.

Mintz, Y., 1982. The sensitivity of numerically simulated climates to land surface conditions. Land Surface Processes in atmospheric general Circulation models 109, 111.

Mintz, Y., Serafini, Y., 1992. A global monthly climatology of soil moisture and water balance. Clim. Dyn. 8 (1), 13–27.

Molini, A., Katul, G.G., Porporato, A., 2009. Revisiting rainfall clustering and intermittency across different climatic regimes. Water Resour. Res. 45 (11) https://doi.org/10.1029/2008WR007352.

Montaldo, N., Oren, R., 2022. Rhizosphere water content drives hydraulic redistribution: implications of pore-scale heterogeneity to modeling diurnal transpiration in water-limited ecosystems. Agric. For. Meteorol. 312, 108720.

Montaldo, N., Albertson, J., Mancini, M., 2008. Vegetation dynamics and soil water balance in a water-limited Mediterranean ecosystem on Sardinia. Italy, Hydrol. Earth System Sci. 12 (6), 1257–1271.

Montaldo, N., Corona, R., Albertson, J.D., 2013. On the separate effects of soil and land cover on Mediterranean ecohydrology: two contrasting case studies in Sardinia, Italy. Water Resour. Res. 49 (2), 1123–1136.

Montaldo, N., Curreli, M., Corona, R., Oren, R., 2020. Fixed and variable components of evapotranspiration in a Mediterranean wild-olive-grass landscape mosaic. Agric. For. Meteorol. 280, 107769.

Montaldo, N., Corona, R., Curreli, M., Sirigu, S., Piroddi, L., Oren, R., 2021. Rock water as a key resource for patchy ecosystems on shallow soils: digging deep tree clumps subsidize surrounding surficial grass. Earth's Future 9 (2) e2020EF001870.

Montaldo, N., Corona, R., Curreli, M., Sirigu, S., Piroddi, L., Oren, R., 2021. Rock water as a key resource for patchy ecosystems on shallow soils: digging deep tree clumps subsidize surrounding surficial grass. Earth's Future 9 (2) e2020EF001870.

Nakai, T., Katul, G.G., Kotani, A., Igarashi, Y., Ohta, T., Suzuki, M., Kumagai, T., 2014. Radiative and precipitation controls on root zone soil moisture spectra. Geophys. Res. Lett. 41 (21), 7546–7554.

Nicolai-Shaw, N., Gudmundsson, L., Hirschi, M., Seneviratne, S.I., 2016. Long-term predictability of soil moisture dynamics at the global scale: persistence versus large-scale drivers. Geophys. Res. Lett. 43 (16), 8554–8562.

Noilhan, J., Planton, S., 1989. A simple parameterization of land surface processes for meteorological models. Mon. Weather Rev. 117 (3), 536–549.

Oglesby, R.J., Marshall, S., Erickson Iii, D.J., Roads, J.O., Robertson, F.R., 2002. Thresholds in atmosphere–soil moisture interactions: Results from climate model studies. J. Geophys. Res.: Atmos. 107 (D14). ACL–15.

Pan, Z., Segal, M., Turner, R., Takle, E., 1995. Model simulation of impacts of transient surface wetness on summer rainfall in the United States Midwest during drought and flood years. Mon. Weather Rev. 123 (5), 1575–1581.

Pan, Z., Arrit, R.W., Gutowski, W.J., Takle, E.S., 2001. Soil moisture in a regional climate model: simulation and projection. Geophys. Res. Letters. ISSN: 00948276 28 (15), 2947–2950. https://doi.org/10.1029/2000GL012172.

Quintana-Seguí, P., Barella-Ortiz, A., Regueiro-Sanfiz, S., Miguez-Macho, G., 2020. The utility of land-surface model simulations to provide drought information in a water management context using global and local forcing datasets. Water Resour. Manage 34 (7), 2135–2156.

Schwingshackl, C., Hirschi, M., Seneviratne, S.I., 2017. Quantifying spatiotemporal variations of soil moisture control on surface energy balance and near-surface air temperature. J. Clim. 30 (18), 7105–7124.

Seneviratne, S.I., Koster, R.D., 2012. A revised framework for analyzing soil moisture memory in climate data: derivation and interpretation. J. Hydrometeorol. 13 (1), 404–412.

Seneviratne, S.I., Corti, T., Davin, E.L., Hirschi, M., Jaeger, E.B., Lehner, I., Orlowsky, B., Teuling, A.J., 2010. Investigating soil moisture–climate interactions in a changing climate: a review. Earth Sci. Rev. 99 (3–4), 125–161.

Shiklamonov, I., 1993. Chapter 2: world fresh water resources, In: Gleick, P.H. (Ed.), Water in Crisis, vol. 9, Pacific Institute for Studies in Dev., Environment & Security. Stockholm Env. Institute, Oxford Univ. Press, pp. 1–24.

Shukla, J., Mintz, Y., 1982. Influence of land-surface evapotranspiration on the earth's climate. Science 215 (4539), 1498–1501.

Siqueira, M., Katul, G., Porporato, A., 2009. Soil moisture feedbacks on convection triggers: the role of soil–plant hydrodynamics. J. Hydrometeorol. 10 (1), 96–112.

Srivastava, A., Saco, P.M., Rodriguez, J.F., Kumari, N., Chun, K.P., Yetemen, O., 2021. The role of landscape morphology on soil moisture variability in semi-arid ecosystems. Hydrol. Process. 35 (1), e13990.

Stoy, P.C., Katul, G.G., Siqueira, M.B., Juang, J.-Y., McCarthy, H.R., Kim, H.-S., Oishi, A. C., Oren, R., 2005. Variability in net ecosystem exchange from hourly to inter-annual time scales at adjacent pine and hardwood forests: a wavelet analysis. Tree Physiol. 25 (7), 887–902.

van den Hurk, B., Doblas-Reyes, F., Balsamo, G., Koster, R.D., Seneviratne, S.I., Camargo, H., 2012. Soil moisture effects on seasonal temperature and precipitation forecast scores in Europe. Clim. Dyn. 38 (1), 349–362.

van Oorschot, F., van der Ent, R.J., Hrachowitz, M., Alessandri, A., 2021. Climate-controlled root zone parameters show potential to improve water flux simulations by land surface models. Earth Syst. Dyn. 12 (2), 725–743.

Vinnikov, K.Y., Robock, A., Speranskaya, N.A., Schlosser, C.A., 1996. Scales of temporal and spatial variability of midlatitude soil moisture. J. Geophys. Res.: Atmos. 101 (D3), 7163–7174.

Wang, A., Zeng, X., Shen, S.S., Zeng, Q.-C., Dickinson, R.E., 2006. Time scales of land surface hydrology. J. Hydrometeorology 7 (5), 868–879.

Wei, J., Dickinson, R.E., Zeng, N., 2006. Climate variability in a simple model of warm climate land-atmosphere interaction. J. Geophys. Res.: Biogeosci. 111 (G3) https://doi.org/10.1029/2005JG000096.

Western, A.W., Grayson, R.B., Blöschl, G., 2002. Scaling of soil moisture: A hydrologic perspective. Annu. Rev. Earth Planet. Sci. 30 (1), 149–180.

Xia, Y., Ek, M.B., Wu, Y., Ford, T., Quiring, S.M., 2015. Comparison of NLDAS-2 simulated and NASMD observed daily soil moisture. Part I: comparison and analysis. J. Hydrometeorol. 16 (5), 1962–1980.

Yeh, T., Wetherald, R.T., Manabe, S., 1984. The effect of soil moisture on the short-term climate and hydrology change–a numerical experiment. Mon. Weather Rev. 112 (3), 474–490.

Yuan, S., Quiring, S.M., 2017. Evaluation of soil moisture in CMIP5 simulations over the contiguous United States using in situ and satellite observations. Hydrol. Earth Syst. Sci. 21 (4), 2203–2218.

Zhou, S., Williams, A.P., Berg, A.M., Cook, B.I., Zhang, Y., Hagemann, S., Lorenz, R., Seneviratne, S.I., Gentine, P., 2019. Land–atmosphere feedbacks exacerbate concurrent soil drought and atmospheric aridity. Proc. Nat. Acad. Sci. 116 (38), 18848–18853.

Zhu, B., Xie, X., Meng, S., Lu, C., Yao, Y., 2020. Sensitivity of soil moisture to precipitation and temperature over China: present state and future projection. Science of The Total Environment 705, 135774.